Gaussian packet prestack depth migration. Part 3: Simple 2-D models

Václav Bucha
Department of Geophysics, Faculty of Mathematics and Physics, Charles University, Ke Karlovu 3, 121 16 Praha 2, Czech Republic, E-mail: bucha@seis.karlov.mff.cuni.cz

Summary

Gaussian packet prestack depth migration is used for calculation of migrated sections in two simple 2-D velocity models. Several improvements of the method have been implemented. We show differences between migrated sections computed with optimized and non-optimized (uniform) Gaussian packets. We compare the migrated sections with the results of Kirchhoff migration.

Keywords

Gaussian packets, Gaussian beams, prestack depth migration, Gabor transform, 2-D velocity model, wave field.

1. Introduction

The paper continues the work described in paper by Bucha (2008) where we expected improvement in the reconstruction of the bottom part of the Marmousi model, but the stacked migrated sections were nearly equal for uniform and optimized Gaussian packets. We decided to perform tests of Gaussian packet prestack depth migration in two simple models with the aim to verify accuracy and efficiency of the method. During the tests, we applied several improvements in the algorithm and the computer code. Reference calculations with Kirchhoff migration method in the same models were performed for comparison.

The algorithm of the Gaussian packet prestack depth migration consists of four basic steps:

a) preparation of a velocity model sufficiently smooth for ray tracing and for application of Gaussian beams and packets,

b) optimization of the shape of Gaussian packets including smoothing,

c) decomposition of the recorded wave field into optimized Gaussian packets,

d) back-propagation of the wave field using Gaussian packets and application of the imaging functional.

We used two simple 2-D velocity models for calculation of the recorded wave field. The models for optimization and migration were homogeneous. We made improvements in the algorithms and computer codes for migration steps b), c) and d).

Updated software (Fortran 77 source codes, data files, history files, descriptions) is included in package DATA (Bucha & Bulant, 2009).

In: Seismic Waves in Complex 3-D Structures, Report 19 (Department of Geophysics, Charles University, Prague, 2009), pp. 39–50

2. 2-D velocity models

To verify accuracy and efficiency of the method and test the improvements, we constructed two simple 2-D models composed of homogeneous blocks. The first model contains horizontal interface and the second model has curved interface. The dimensions of the models and measurement configuration were taken from the Marmousi model and dataset (Versteeg & Grau, 1991).

The first model is composed of two homogeneous velocity blocks separated by one horizontal interface located at the depth of 2.4 km (see Figure 1). The upper block has P-wave velocity $V_p = 2.5$ km/s, and the bottom block $V_p = 3.6$ km/s.

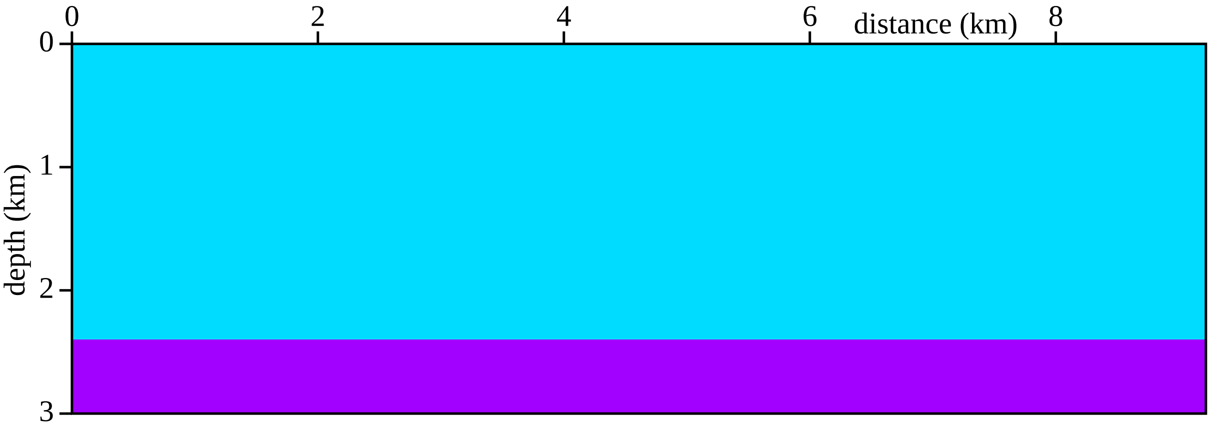

Figure 1. Model with horizontal interface.

The second model is derived from the 3-D Salt dome model (SD1) (for details see Klimeš, 1995) that can be found in SW3D package DATA (Bucha & Bulant, 2009). The model is composed of two homogeneous velocity blocks separated by one curved interface (see Figure 2). The upper block has P-wave velocity $V_p = 2.5$ km/s, and the velocity in the salt dome is $V_p = 4.4$ km/s. S-wave velocity in both models is $V_s = V_p/\sqrt{3}$, density is $\rho = 1$, P and S-wave loss factors are $Q_p^{-1} = 0$ and $Q_s^{-1} = 0$.

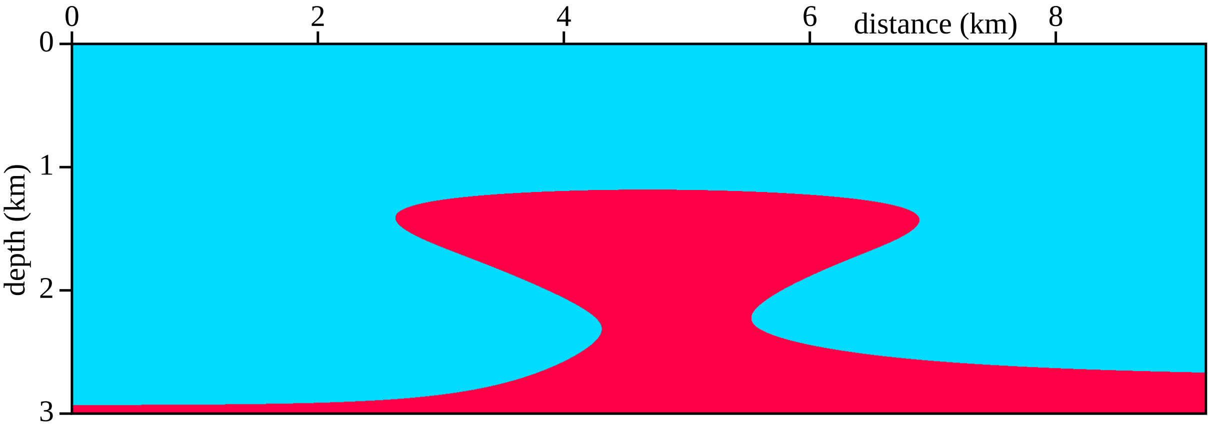

Figure 2. Model with curved interface.

For migrations, we used homogeneous models with material parameters corresponding to the upper blocks, i.e., with P-wave velocity $V_p = 2.5$ km/s in both cases.

3. Recorded wave field

Computation of the recorded wave field in the two simple models was performed using the MODEL, CRT and FORMS subroutine packages (Červený, Klimeš & Pšenčík, 1988). The measurement configuration was the same as the Marmousi model and dataset (Versteeg & Grau, 1991): the first shot was at 3 km, the last shot was at 8.975 km, distance between shots was 0.025 km, number of traces per shot was 96, the first trace was at offset 2.575 km left of shot location, the last trace was at offset 0.2 km left of shot location, the distance between traces was 0.025 km, the sampling interval was 4 ms and the number of samples per trace was 750. The total number of shots was 240.

Ray-theory seismograms were computed for all 240 shot-receiver configurations. Two-point rays were calculated for reflected P-wave in the model with horizontal interface. Three elementary reflected P-waves were computed in the model with curved interface. P-wave reflections from outside and inside of the curved interface were calculated.

4. Optimization of the shape of Gaussian packets

The envelope of optimized Gaussian packets, in the plane perpendicular to the central ray of the packet, depends not only on the frequency ω, but also on the coordinate x_{R} of the intersection of the central ray of a Gaussian packet with the profile, on its arrival time t_{R}, and on the component p of the slowness vector along the profile. Parameter $N^0(x_{\mathrm{R}}, t_{\mathrm{R}}, p)$ describes the shape of a corresponding Gaussian beam along the initial surface. Imaginary part $\mathrm{Im}(N^0)$ determines the Gaussian beam width and real part $\mathrm{Re}(N^0)$ defines the curvature of the wavefront. Since we are using axially symmetric Gaussian packets, and thus need to control their spreading in the plane perpendicular to the central ray of the packet, it is sufficient to optimize the initial shape of corresponding Gaussian beams (Žáček, 2005).

Whereas Žáček (2006a) smoothed the optimized values of N^0, we switched to smoothing the optimized values of $1/N^0$ (Bucha, 2008) that is more stable for computation. The modified equations derived by Klimeš have not been published yet. Values of the optimum shape of parameters $\mathrm{Re}(N^0)$ and $\mathrm{Im}(N^0)$ were analytically verified with success for the homogeneous model using eq. 23 by Klimeš (2008).

Smoothing of the optimized values was equal in all three directions of coordinates x_{R}, t_{R} and p along the Hamiltonian hypersurface. The value of the smoothing parameter was constant for all 240 shots because we used a homogeneous model.

Figures 3, 4 show examples of distribution of parameter $\mathrm{Im}(N^0)$ calculated for shot 120 (at a horizontal coordinate of 5.975 km). Figure 3 shows the optimized values and Figure 4 shows the optimized values smoothed into the range of approximately two orders of magnitude.

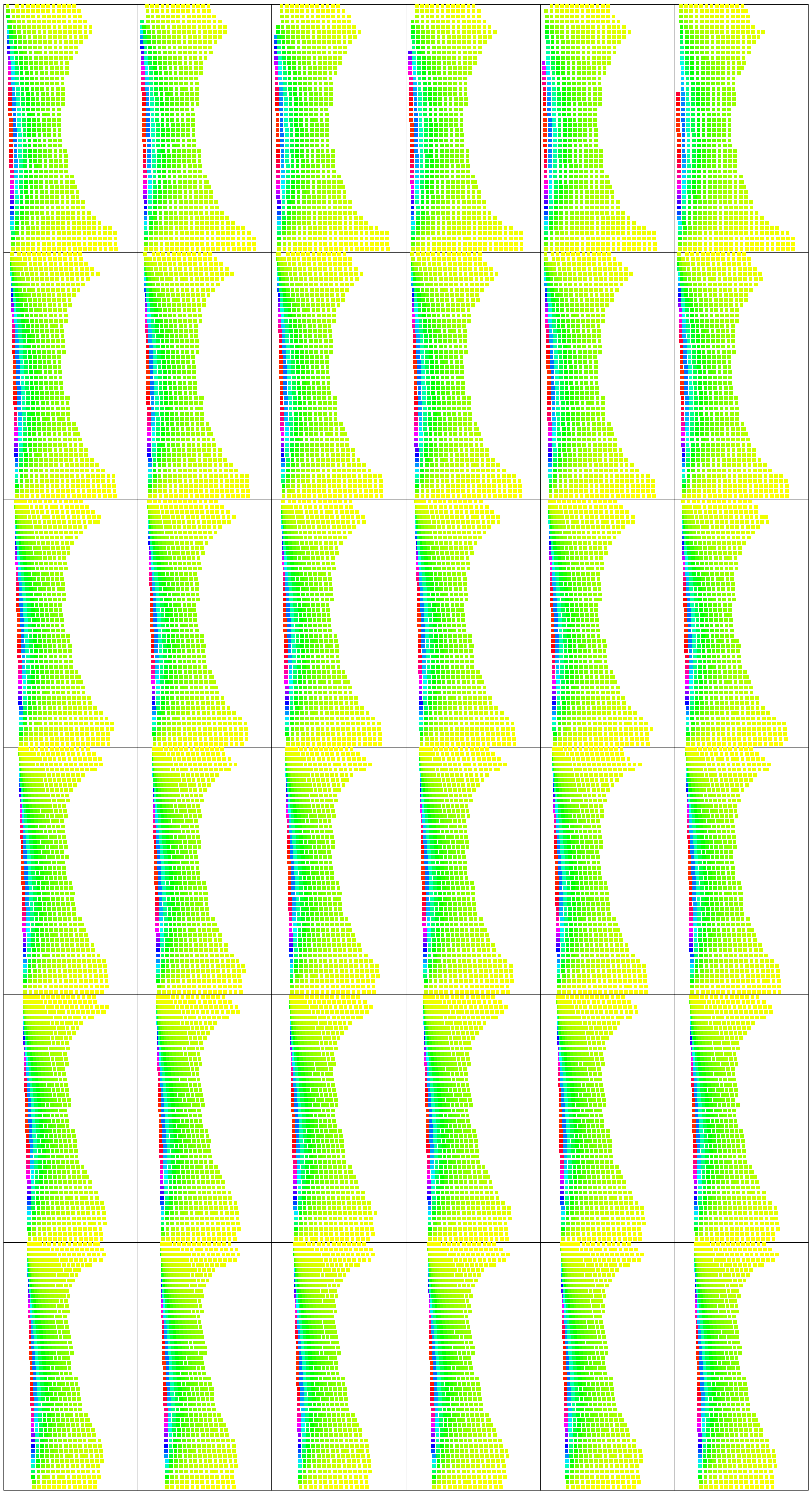

Figure 3. Distribution of the optimized initial parameter $\mathrm{Im}(N^0(x_\mathrm{R}, t_\mathrm{R}, p))$ on the Hamiltonian hypersurface for shot 120 (at a horizontal coordinate of 5.975 km). Left bottom distribution corresponds to the first, and right top distribution to the last of 36 discrete values of x_R. Left bottom corner of each distribution corresponds to the minimum values of t_R and p. t_R increases horizontally and p increases vertically for each of 36 distributions. Colour scale: yellow corresponds to $\mathrm{Im}(N^0) = 0.2 \times 10^{-8}\ \mathrm{s\,m^{-2}}$, green corresponds to $\mathrm{Im}(N^0) = 0.27 \times 10^{-6}\ \mathrm{s\,m^{-2}}$ and red corresponds to $\mathrm{Im}(N^0) = 0.13 \times 10^{-5}\ \mathrm{s\,m^{-2}}$.

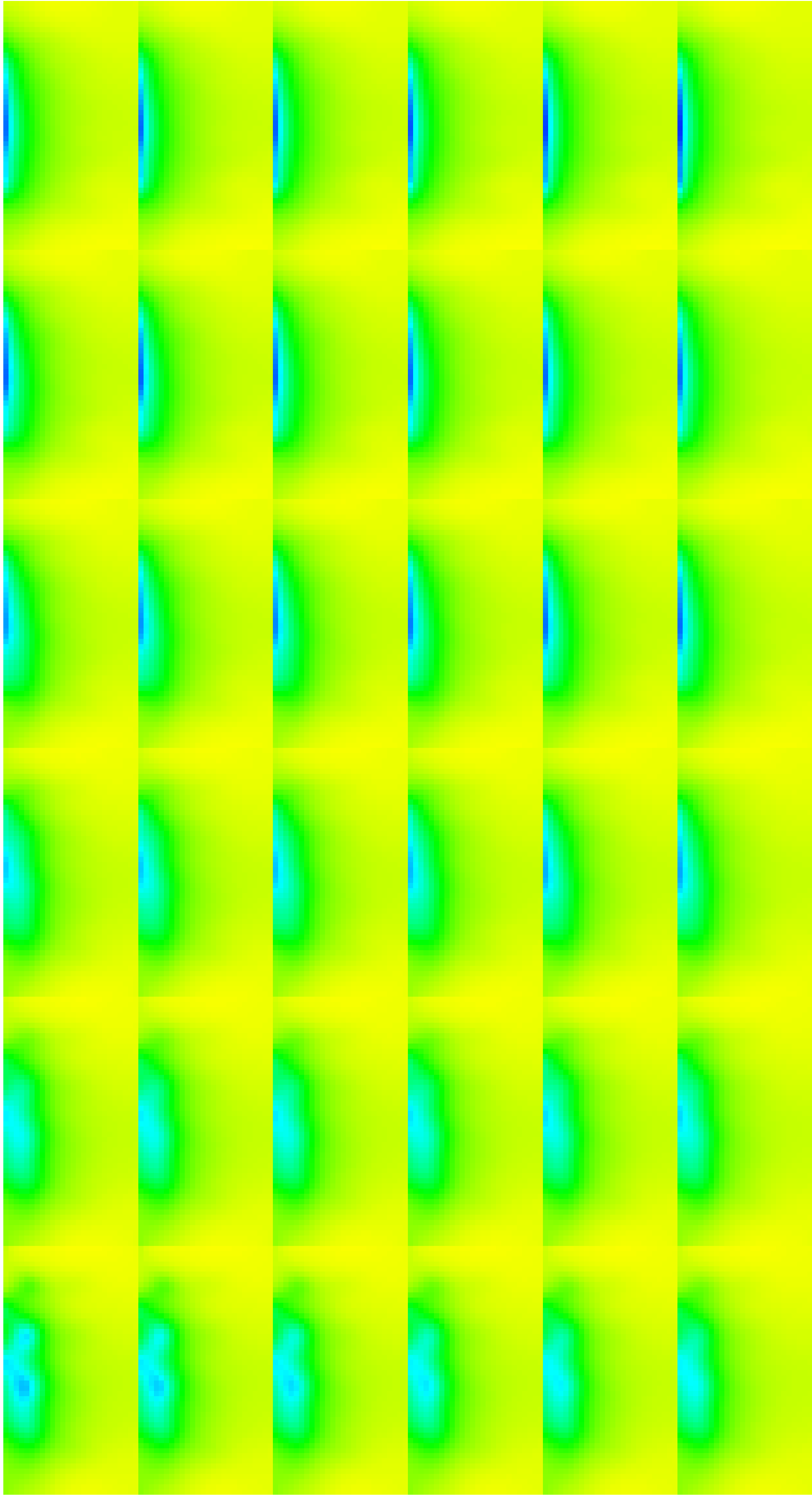

Figure 4. Distribution of the optimized and smoothed initial parameter $\mathrm{Im}(N^0(x_\mathrm{R}, t_\mathrm{R}, p))$ on the Hamiltonian hypersurface for shot 120 (at a horizontal coordinate of 5.975 km). The smoothed values vary in *two* orders of magnitude. Left bottom distribution corresponds to the first, and right top distribution to the last of 36 discrete values of x_R. Left bottom corner of each distribution corresponds to the minimum values of t_R and p. t_R increases horizontally and p increases vertically for each of 36 distributions. Colour scale: yellow corresponds to $\mathrm{Im}(N^0) = 0.2 \times 10^{-8}\ \mathrm{s\,m^{-2}}$, green corresponds to $\mathrm{Im}(N^0) = 0.27 \times 10^{-6}\ \mathrm{s\,m^{-2}}$, and blue corresponds to $\mathrm{Im}(N^0) = 0.8 \times 10^{-6}\ \mathrm{s\,m^{-2}}$.

5. Decomposition of the recorded wave field into optimized Gaussian packets

For computation of maximum discretization steps $\Delta x_{\rm R}$ and $\Delta t_{\rm R}$, Žáček (2003) used his equations (38), (40):

$$\Delta x_{\rm R} \approx \kappa \sqrt{-\frac{2(1-\nu)}{\omega_{\rm MAX}} \mathrm{Im}\left[\frac{\left(1-\frac{\mathrm{i}\ \mathrm{Im}(N_{\rm MIN})}{N_{\rm MAX}}\frac{\omega_{\rm MIN}}{\omega_{\rm MAX}}\xi\right)}{N_{\rm MAX}}\right]} \quad , \tag{38}$$

$$\Delta t_{\rm R} \approx \kappa \sqrt{-2\nu \mathrm{Im}\left[\frac{\left(1-\frac{\mathrm{i}\ \mathrm{Im}(N_{\rm MIN})}{N_{\rm MIN}}\xi\right)}{K_0}\right]} \quad . \tag{40}$$

Instead, we applied directly equations (45) and (46) by Žáček (2006b):

$$\Delta x_{\rm R} = \kappa \sqrt{-\frac{2}{\omega}\left[\mathrm{Im}\left((\mathbf{K}+\widetilde{\mathbf{K}})^{-1}\right)\right]_{11}} \quad , \tag{45}$$

$$\Delta t_{\rm R} = \kappa \sqrt{-\frac{2}{\omega}\left[\mathrm{Im}\left((\mathbf{K}+\widetilde{\mathbf{K}})^{-1}\right)\right]_{22}} \quad . \tag{46}$$

This change was applied in computer codes for calculation of discretization steps (program `gpstep.for`) and decomposition of the recorded wave field (program `gpanal.for`).

In order to speed up the migration, we added replacing of the smallest amplitudes of Gaussian packets by zeroes. We replaced by zeroes amplitudes F which satisfy inequality (Klimeš, personal communication):

$$\frac{2\pi^3\ \Delta x_{\rm R}\Delta t_{\rm R}\Delta p\Delta\omega}{\mathtt{NX}\ \mathtt{NT}\ \Delta x\Delta t\ \mathtt{GRDNEW}^2}\sum\frac{|F|^2}{\omega^2\sqrt{\mathrm{Im}N\ \mathrm{Im}N_{44}}} \le \mathtt{RELERR}^2 \quad , \tag{1}$$

where

- $\Delta x_{\rm R}$,$\Delta t_{\rm R}$,Δp and $\Delta\omega$ are dicretization steps of the coordinate $x_{\rm R}$ of the intersection of the central ray of a Gaussian packet with the profile, of its arrival time $t_{\rm R}$, of the component p of the slowness vector along the profile and of the frequency ω,
- F is the complex–valued amplitude of the Gaussian packet,
- `NX` is the number of receivers, `NT` is the number of samples in a seismogram, Δx is the distance between receivers, Δt is the sampling interval,
- `GRDNEW` is the L_2 norm of the recorded wave field,
- complex valued parameter N determines initial shape of Gaussian packets and parameter N_{44} is defined by equation (31) in Žáček (2006b),
- `RELERR` is a numerical parameter approximately proportional to the relative root mean square error of the seismograms caused by replacing the smallest amplitudes of Gaussian packets by zeroes. We put `RELERR` equal to the desired relative error, calculate the actual relative error and update `RELERR`.

To apply the changes, the program `gpanal.for` was split into two parts. The first part computes decomposition of the recorded wave field (program `gpanal.for`) and the second part performs replacing of the smallest amplitudes of Gaussian packets by zeroes and computes composition of the approximated wave field (program `gpsynt.for`).

One of the criteria of usability of smoothed optimized Gaussian packets is the result of decomposition of the recorded wave field for each shot. The differences between the decomposed original wave field and composed approximated wave field should not be significant. Figure 5 shows examples of wave field differences for shot 120 (at a horizontal coordinate of 5.975 km) for non-optimized (uniform) and optimized Gaussian packets for two simple models. The wave field differences seem to be acceptable for both, uniform and optimized Gaussian packets.

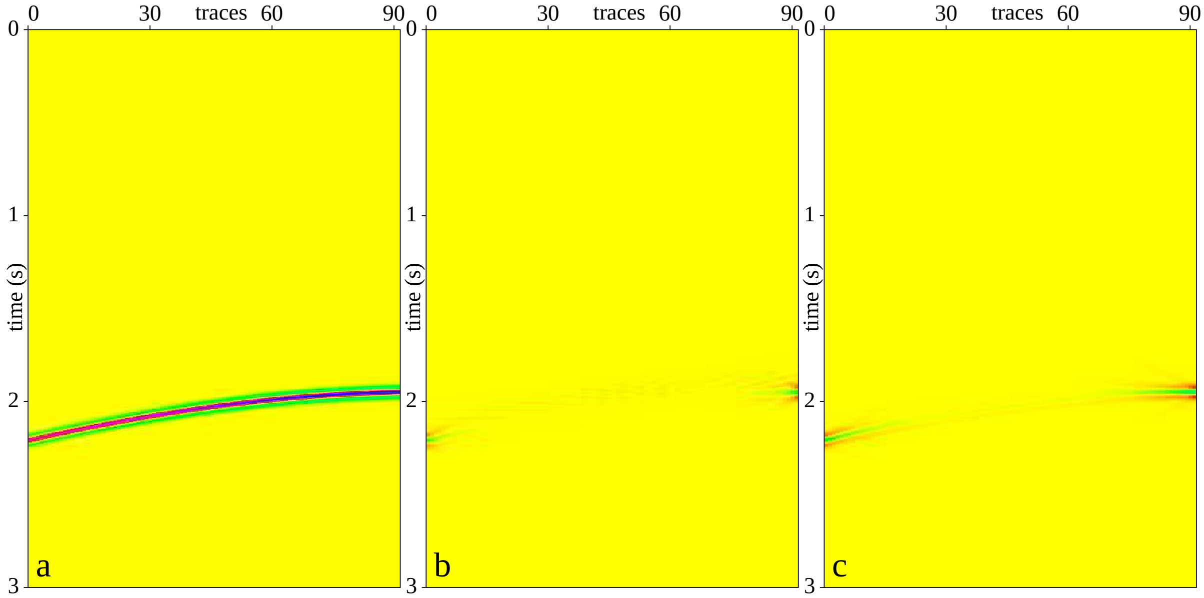

Model with horizontal interface

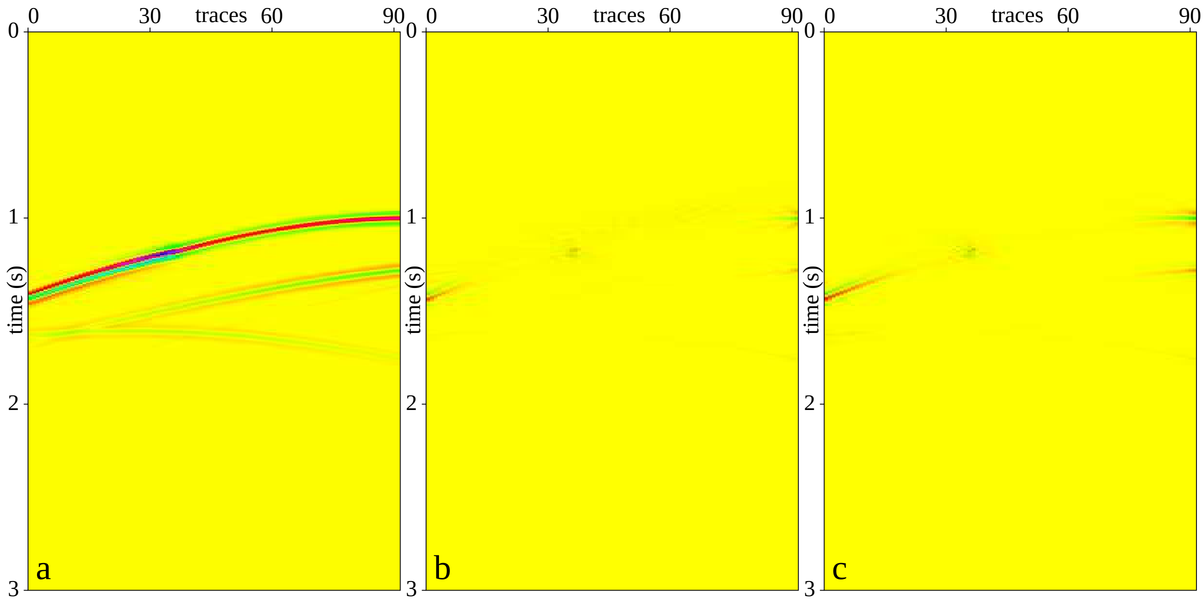

Model with curved interface

Figure 5. Examples of wave field differences for a shot 120 (at a horizontal coordinate of 5.975 km) in the model with horizontal interface (the first row) and in the model with curved interface (the second row): (a) Recorded wave field, (b) differences between original wave field and approximated wave field for non-optimized Gaussian packets, (c) differences between original wave field and approximated wave field for optimized Gaussian packets with $\mathrm{Im}(N^0)$ differing by *two* orders of magnitude. Colour scale is identical for all figures in each row: from yellow that corresponds to zero, up to red that corresponds to the maximum amplitude.

6. Migration

The migration was computed in the homogeneous model with P-wave velocity $V_p = 2.5$ km/s, the same velocity as we used in the upper blocks of two simple models. Figures 6, 7 display two simple models and stacked migrated sections. Figures 6b, 7b display results of Gaussian packet migration computed using uniform Gaussian packets. Figures 6c, 7c show stacked migrated sections calculated using smoothly optimized (non-uniform) Gaussian packets. The range of $\mathrm{Im}(N^0)$ (ratio of $[\mathrm{Im}(N^0)]_{\mathrm{MAX}}$ to $[\mathrm{Im}(N^0)]_{\mathrm{MIN}}$) was approximately two orders of magnitude. The differences between the use of uniform and optimized Gaussian packets are very small.

Let us mention that some parts of the curved interface are not at the right position. It is caused by rays of reflected P-waves traced through the salt block with different velocity than the homogeneous model.

We sped up migration approximately three times at a very small expense of accuracy. The following steps were used:

- we increased the ratio of the step between two subsequent beams to their characteristic half-width (parameter KAPPA),
- we increased relative decay of the Gaussian envelope at which the loop over the points of the seismograms is terminated (parameter RELAMP) and
- we replaced the smallest amplitudes of Gaussian packets by zeroes (parameter RELERR, performed in decomposition).

We added for comparison the stacked migrated sections calculated using the Kirchhoff migration (see Figures 6d, 7d). The efficiency of this method is much better than of the Gaussian packet migration. The time of the Kirchhoff migration, computed on a grid of cells 16×16 metres and interpolated to grid of cells 4×4 metres, is approximately 100 minutes. The Gaussian packet migration was computed on a grid of cells 20×20 metres and interpolated to grid of cells 4×4 metres. The time of the Gaussian packet migration with uniform packets is approximately 2 days, the time of the Gaussian packet migration with optimized packets with $\mathrm{Im}(N^0)$ differing by two orders of magnitude is approximately 1 month. The times of the computation correspond to an Athlon one core 2.3 GHz processor.

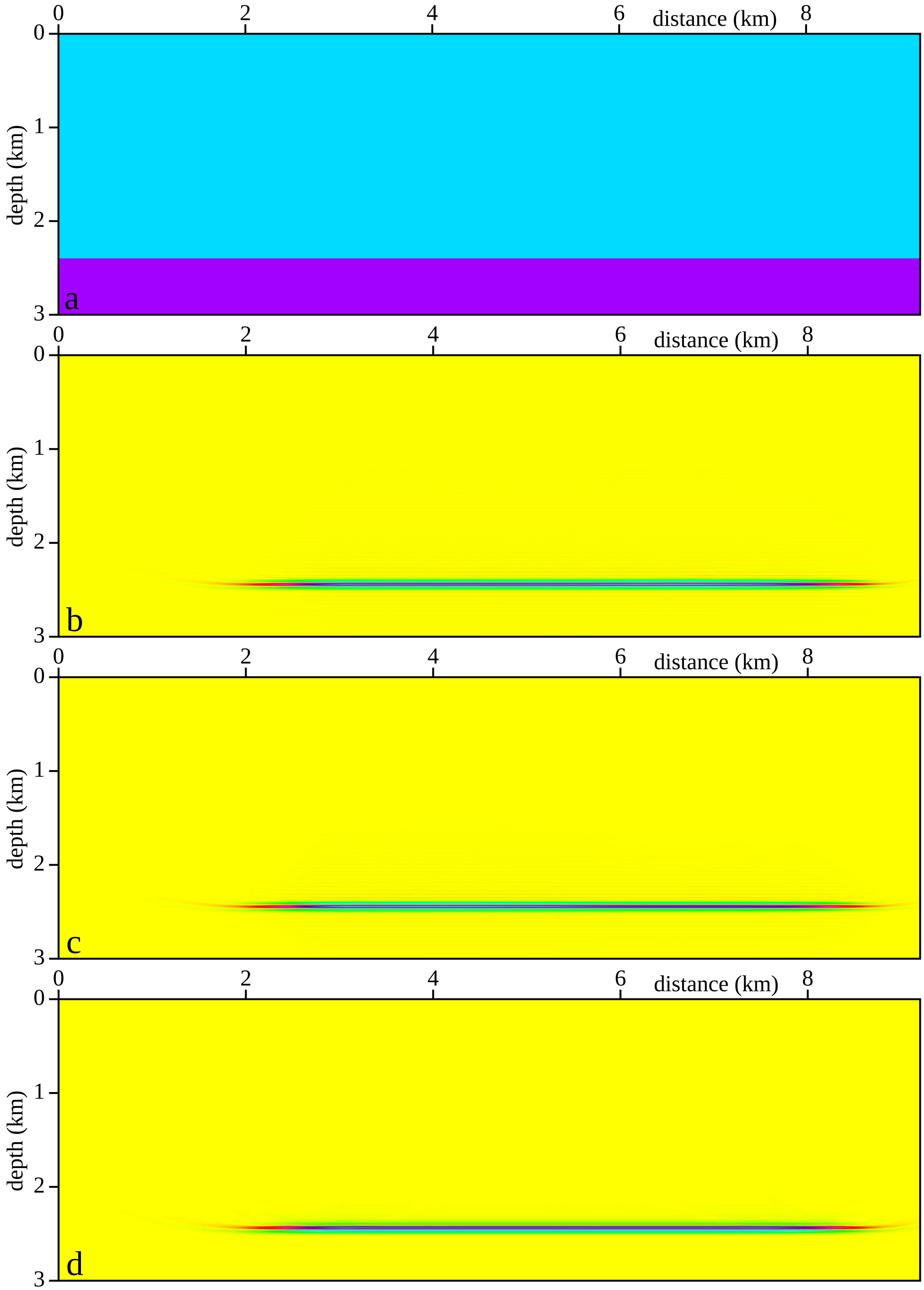

Figure 6. **(a) Model with horizontal interface, (b) Gaussian packet migration with uniform $\mathrm{Im}(N^0)$, (c) Gaussian packet migration with $\mathrm{Im}(N^0)$ differing by *two* orders of magnitude, (d) Kirchhoff migration.**

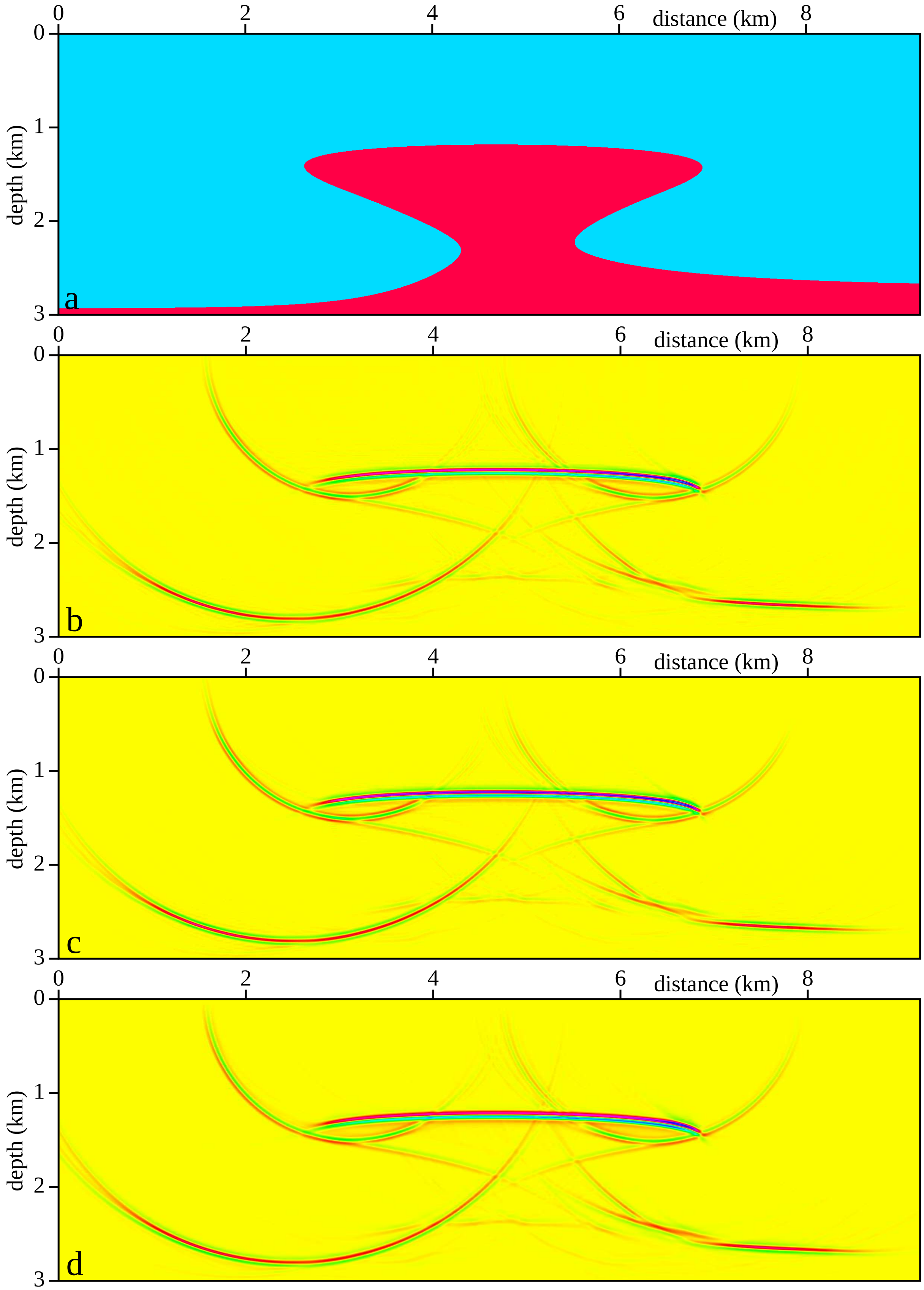

Figure 7. (a) Model with curved interface, (b) Gaussian packet migration with uniform $\mathrm{Im}(N^0)$, (c) Gaussian packet migration with $\mathrm{Im}(N^0)$ differing by *two* orders of magnitude, (d) Kirchhoff migration.

7. Conclusions

We used Gaussian packet prestack depth migration for calculation of migrated sections in two simple 2-D velocity models. In two presented examples, the differences between migrated sections computed with optimized and non-optimized (uniform) Gaussian packets are very small. Non-optimized Gaussian packets seem to be sufficient for computation in simple 2-D velocity models composed of homogeneous velocity blocks.

Comparison of migrated sections calculated with Kirchhoff migration and Gaussian packet migration showed also very small differences. Although we again sped up the Gaussian packet migration, computations indicate that the Kirchhoff migration is incomparably faster.

Acknowledgments

The author thanks Luděk Klimeš for valuable comments and recommendations concerning this paper, and for his assistance with improvements of the algorithm and Karel Žáček's computer codes for the Gaussian packet migration.

The research has been supported by the Grant Agency of the Czech Republic under contract 205/07/0032, by the Ministry of Education of the Czech Republic within research project MSM0021620860, and by the members of the consortium "Seismic Waves in Complex 3-D Structures" (see "http://sw3d.cz").

References

Bucha, V. (2008): Gaussian packet prestack depth migration. Part 2: Optimized Gaussian packets. In: Seismic Waves in Complex 3-D Structures, Report 18, pp. 129–138, Dep. Geophys., Charles Univ., Prague, online at "http://sw3d.cz".

Bucha, V. & Bulant, P. (eds.) (2009): SW3D-CD-13 (DVD-ROM). In: Seismic Waves in Complex 3-D Structures, Report 19, pp. 263–264, Dep. Geophys., Charles Univ., Prague, online at "http://sw3d.cz".

Červený, V., Klimeš, L. & Pšenčík, I. (1988): Complete seismic-ray tracing in three-dimensional structures. In: Doornbos, D.J.(ed.), Seismological Algorithms, Academic Press, New York, pp. 89–168.

Klimeš, L. (1995): Examples of seismic models. In: Seismic Waves in Complex 3-D Structures, Report 3, pp. 5–35, Dep. Geophys., Charles Univ., Prague, online at "http://sw3d.cz".

Klimeš, L. (2008): Optimization of the structural Gabor functions in a homogeneous velocity model for a zero-offset surface seismic reflection survey. In: Seismic Waves in Complex 3-D Structures, Report 18, pp. 115–127, Dep. Geophys., Charles Univ., Prague, online at "http://sw3d.cz".

Žáček, K. (2003): Decomposition of the wave field into optimized Gaussian packets. In: Seismic Waves in Complex 3-D Structures, Report 13, pp. 35–43, Dep. Geophys., Charles Univ., Prague, online at "http://sw3d.cz".

Žáček, K. (2005): Gaussian packet prestack depth migration. In: Seismic Waves in Complex 3-D Structures, Report 15, pp. 29–48, Dep. Geophys., Charles Univ., Prague, online at "http://sw3d.cz".

Žáček, K. (2006a): Optimization of the shape of Gaussian beams. Stud. geophys. geod., **50**, 349–366.

Žáček, K. (2006b): Decomposition of the wave field into optimized Gaussian packets. Stud. geophys. geod., **50**, 367–380.